Inorg. Chem. **2006**, *45*, 8862–8875

Structure–Function Correlations in Iron(II) Tris(pyrazolyl)borate Spin-State Crossover Complexes

Daniel L. Reger,* James R. Gardinier,[#] J. Derek Elgin, and Mark D. Smith

Department of Chemistry and Biochemistry, University of South Carolina, Columbia, South Carolina 29208

Dimitri Hautot and Gary J. Long*

Department of Chemistry, University of Missouri—Rolla, Rolla, Missouri 65409-0010

Fernande Grandjean

Department of Physics, B5, University of Liège, B-4000 Sart-Tilman, Belgium

Received May 1, 2006

Iron(II) poly(pyrazolyl)borate complexes have been investigated to determine the impact of substituent effects, intramolecular ligand distortions, and intermolecular supramolecular structures on the spin-state crossover (SCO) behavior. The molecular structure of $Fe[HB(3,4,5\text{-}Me_3pz)_3]_2$ (pz = pyrazolyl ring), a complex known to remain high spin when the temperature is lowered, reveals that this complex has an intramolecular ring-twist distortion that is not observed in analogous complexes that do exhibit a SCO at low temperatures, thus indicating that this distortion greatly influences the properties of these complexes. The structure of $Fe[B(3\text{-}^{cy}Prpz)_4]_2\cdot(CH_3OH)$ (^{cy}Pr = cyclopropyl ring) at 294 K has two independent molecules in the unit cell, both of which are high spin; only one of these high-spin iron(II) sites, the site with the lesser ring-twist distortion, is observed to be low-spin iron(II) in the 90 K structure. A careful evaluation of the supramolecular structures of these complexes and several similar complexes reported previously revealed no strong correlation between the supramolecular packing forces and their SCO behavior. Magnetic and Mössbauer spectral measurements on $Fe[B(3\text{-}^{cy}Prpz)_4]_2$ and $Fe[HB(3\text{-}^{cy}Prpz)_3]_2$ indicate that both complexes exhibit a partial SCO from fully high-spin iron(II) at higher temperatures, respectively, to a 50:50 high-spin/low-spin mixture of iron(II) below 100 K. These results may be understood, in the former case, by the differences in ring-twisting and, in the latter case, by a phase transition; in all complexes in which a phase transition is observed, this change dominates the SCO behavior. A comparison of the Mössbauer spectral properties of these two complexes and of $Fe[HB(3\text{-}Mepz)_3]_2$ with that of other complexes reveals correlations between the Mössbauer-effect isomer shift and the average Fe–N bond distance and between the quadrupole splitting and the average FeN–NB intraligand dihedral torsion angles and the distortion of the average N–Fe–N intraligand bond angles.

Introduction

Octahedral iron(II) complexes that undergo a spin-state crossover (SCO) between the highly colored low-spin $^1A_1$ ($t_{2g}^6e_g^{*0}$) state and the typically colorless or lightly colored high-spin $^5T_2$ ($t_{2g}^4e_g^{*2}$) state[1] have potential applications as 'intelligent' contrast agents for biomedical imaging,[2] as temperature/pressure threshold indicators, and as optical elements in display devices.[3] SCO iron(II) complexes that contain the FeN_6 coordination environment are, by far, the most studied for these applications. Thus, the SCO behavior

* To whom correspondence should be addressed. E-mail: reger@mail.chem.sc.edu (D.L.R.); glong@umr.edu (G.J.L.).

[#] Present address: Department of Chemistry, Marquette University, Milwaukee, WI 53201-1881.

(1) (a) Real, J. A.; Gaspar, A. B.; Niel, V.; Muñoz, M. C. *Coord. Chem. Rev.* **2003**, *236*, 121. (b) Gütlich, P.; Garcia, Y.; Goodwin, H. A. *Chem. Soc. Rev.* **2000**, *29*, 419. (c) Gütlich, P.; Hauser, A.; Spiering, H. *Angew. Chem., Int. Ed. Engl.* **1994**, *33*, 2024. (d) König, E.; Ritter, G.; Kulshreshtha, S. K. *Chem. Rev.* **1985**, *85*, 219.

(2) Muller, R. N.; Van der Elst, L.; Laurent, S. *J. Am. Chem. Soc.* **2003**, *125*, 8405.

(3) Kahn, O.; Martinez, C. J. *Science* **1998**, *279*, 44.

10.1021/ic0607437 CCC: $33.50
Published on Web 08/01/2006

of iron(II) derivatives of triazoles,[4] tetrazoles,[5] isoxazoles,[6] polypyridyls,[7] picolylamines,[8] cyanopyridines,[9] poly(pyrazolyl)borates,[10] and some pyrazolyl/pyridyl mixed-ligand complexes[11] has been reported. One goal of this research is to discover ways to control the SCO behavior such that materials with determined properties can be designed for different, specific applications. Unfortunately, the field of engineering SCO materials is still in its infancy, and although new systems are still being discovered, relatively fewer systematic studies aimed at elucidating both molecular *and* supramolecular aspects of SCO behavior have emerged.[12]

Iron(II) SCO complexes with the tris(pyrazolyl)methane and the tris(pyrazolyl)borate ligands, two common classes of scorpionate ligands,[13] are promising because they permit a systematic study of the influence of ligand substitution upon the SCO behavior. This promise is facilitated by the synthetic simplicity of, and nearly endless possibilities for, modification of the scorpionate backbone.[13] The SCO behavior of these iron(II) scorpionates has been the subject of a recent review.[14] Since publication of this review, some of us have reported interesting new observations regarding the differing SCO behavior for polymorphs of $Fe[(p\text{-}IC_6H_4)B(3\text{-}Mepz)_3]_2$ (pz = pyrazolyl ring)[15] and of derivatives in which the iodide group is substituted by designed organic groups, such as in $Fe[(p\text{-}PhC{\equiv}CC_6H_4)B(3\text{-}Mepz)_3]_2$.[16] One goal of these studies was to demonstrate that, by manipulating the crystal packing environment of very similar (or even the same) iron(II) complexes, the SCO behavior could be fine-tuned. Thus, it was found that noncovalent interactions, such as $\pi-\pi$, CH$\cdots\pi$, and other weak hydrogen-bonding interactions, such as CH−halide interactions, provided a means for controlling the SCO temperature and could even be exploited to prevent the crossover from occurring at low temperatures. In addition, the earlier work[16] demonstrated that in $Fe[(p\text{-}HC{\equiv}CC_6H_4)B(3\text{-}Mepz)_3]_2$, which has two crystallographically independent but supramolecularly similar molecules per unit cell, ligand distortions, such as twisting of the pyrazolyl rings, can play a critical role in determining the temperature at which SCO occurs.

With these observations in mind, we have re-examined the SCO behavior of many related iron(II) poly(pyrazolyl)borate complexes in greater detail with respect to the substituents effects,[17] ligand distortions,[18] and supramolecular structures both to determine whether any trends emerge and to answer some important current questions. For example, why are the magnetic properties[14,19] of $Fe[HB(3,4,5\text{-}Me_3pz)_3]_2$ so different from those of $Fe[HB(3,5\text{-}Me_2pz)_3]_2$? That is, why does the former complex remain fully high spin down to 1.7 K whereas the latter changes to low-spin at approximately 190 K? Are there any unusual molecular or supramolecular structural features of this complex that may readily explain this difference and the other related differences in this class of complexes? As part of this contribution, we have examined the variable-temperature structural, magnetic, and Mössbauer spectral properties of a number of known complexes that have not been previously studied in detail. Such studies have allowed us to make the interesting structure−function correlations that are reported below. It is also hoped that the findings reported herein will inspire further advances in ligand design and crystal engineering of new SCO complexes based on iron(II) scorpionates.

(4) (a) Roubeau, O.; Gomez, J. M. A.; Balskus, E.; Kolnaar, J. J. A.; Haasnoot, J. G.; Reedjik, J. *New. J. Chem.* **2001**, *25*, 144. (b) Kolnaar, J. J. A.; De Heer, M. I.; Kooijman, H.; Spek, A. L.; Schmitt, G.; Ksenofontov, V.; Gütlich, P.; Haasnoot, J. G.; Reedijk, J. *Eur. J. Inorg. Chem.* **1999**, *5*, 881. (c) Garcia, Y.; van Koningsbruggen, P. J.; Codjovi, E.; Lapouyade, R.; Kahn, O.; Rabardel, L. *J. Mater. Chem.* **1997**, *7*, 857.

(5) (a) Grunert, C. M.; Schweifer, J.; Weinberger, P. W.; Linert, W.; Mereiter, K.; Hilscher, G.; Muller, M.; Wiesinger, G.; van Koningsbruggen, P. J. *Inorg. Chem.* **2004**, *43*, 155. (b) Stassen, A. F.; Roubeau, O.; Ferrero Gramage, I.; Linares, J.; Varret, F.; Mutikainen, I.; Turpeinen, U.; Haasnoot, J. G.; Reedijk, J. *Polyhedron* **2001**, *20*, 1699.

(6) Hibbs, W.; van Koningsbruggen, P. J.; Arif, A. M.; Shum, W. W.; Miller, J. S. *Inorg. Chem.* **2003**, *42*, 5645.

(7) (a) Moliner, N.; Muñoz, M. C.; Letard, S.; Salmon, L.; Tuchagues, J.-P.; Bousseksou, A.; Real, J. A. *Inorg. Chem.* **2002**, *41*, 6997. (b) Moliner, N.; Salmon, L.; Capes, L.; Muñoz, M. C.; Tuchagues, J.-P.; Bousseksou, A.; McGarvey, J. J.; Dennis, A. C.; Castro, M.; Burriel, R.; Real, J. A. *J. Phys. Chem. B* **2002**, *106*, 4276. (c) Real, J. A.; Muñoz, M. C.; Faus, J.; Solans, X. *Inorg. Chem.* **1997**, *36*, 3008. (d) Müller, E. W.; Spiering, H.; Gütlich, P. *Chem. Phys. Lett.* **1982**, *93*, 567. (e) König, E.; Madeja, K.; Watson, K. J. *J. Am. Chem. Soc.* **1968**, *90*, 1146.

(8) Spiering, H.; Meissner, E.; Köppen, H.; Müller, E. W.; Gütlich, P. *Chem. Phys.* **1982**, *68*, 65.

(9) Galet, A.; Niel, V.; Muñoz, M. C.; Real, J. A. *J. Am. Chem. Soc.* **2003**, *125*, 14227.

(10) (a) Oliver, J. D.; Mullica, D. F.; Hutchinson, B. B.; Milligan, W. O. *Inorg. Chem.* **1980**, *19*, 195. (b) Jesson, J. P., Trofimenko, S.; Eaton, D. R. *J. Am. Chem. Soc.* **1967**, *89*, 3158. (c) Jesson, J. P.; Weiher, J. F. *J. Chem. Phys.* **1967**, *46*, 1995. (d) Jesson, J. P.; Weiher, J. F.; Trofimenko, S. *J. Chem. Phys.* **1968**, *48*, 2058.

(11) (a) Leita, B. A.; Moubaraki, B.; Murray, K. S.; Smith, J. P.; Cashion, J. D. *Chem. Commun.* **2004**, 156. (b) Sugiyarto, K. H.; McHale, W.-A.; Craig, D. C.; Rae, A. D.; Scudder, M. L.; Goodwin, H. A. *Dalton Trans.*, **2003**, 2443. (c) Manikandan, P.; Padmakumar, K.; Thomas, K. R. J.; Varghse, B.; Onodera, H.; Manoharan, P. T. *Inorg. Chem.* **2001**, *40*, 6930. (d) Holand, J. M.; McAllister, J. A.; Lu, Z.; Kilner, C. A.; Thornton-Pett, M.; Halcrow, M. A. *Chem. Commun.* **2001**, 577. (e) Suemara, N.; Ohama, M.; Kaizaki, S. *Chem. Comm*. **2001**, 1538.

(12) See for example: (a) Ksenofontov, V.; Gaspar, A. B.; Levchenko, G.; Fitzsimmons, B.; Gütlich, P. *J. Phys. Chem. B* **2004**, *108*, 7723. (b) Thompson, A. L.; Goeta, A. E.; Real, J. A.; Galet, A.; Muñoz, M. C. *Chem. Commun* **2004**, 1390. (c) Marchivie, M.; Guionneau, P.; Létard, J.-F.; Chasseau, D. *Acta Crystallogr.* **2003**, *B59*, 479. (d) Matouzenko, G. S.; Bousseksou, A.; Lecocq, S.; van Koningsbruggen, P. J.; Perrin, M.; Kahn, O.; Collet, A. *Inorg. Chem.* **1997**, *36*, 5869. (e) Sugiyarto, K. H.; Craig, D. C.; Goodwin, H. A. *Aust. J. Chem.* **1996**, *49*, 497. (f) Konno, M.; Mikami-Kido, M. *Bull. Chem. Soc. Jpn.* **1991**, *64*, 339. (g) Ozarowski, A.; McGarvey, B. R.; Sarkar, A. B.; Drake, J. E. *Inorg. Chem.* **1988**, *27*, 628. (h) König, E.; Madeja, K.; Watson, K. J. *J. Am. Chem. Soc.* **1968**, *90*, 1146. (i) König, E.; Madeja, K. *Inorg. Chem.* **1967**, *6*, 48. (j) Guionneau, P.; Létard, J.-F.; Yufit, D. S.; Chasseau, D.; Bravic, G.; Goeta, A. E.; Howard, J. A. K.; Kahn, O. *J. Mater. Chem.* **1999**, *9*, 985.

(13) (a) Trofimenko, S. *J. Am. Chem. Soc.* **1966**, *88*, 1842. (b) Trofimenko, S. *Scorpionates: The Coordination Chemistry of Polypyrazolylborate Ligands*; Imperial College Press: London, 1999.

(14) Long, G. J.; Grandjean, F.; Reger, D. L. In *Spin Crossover in Transition Metal Compounds I*; Gütlich, P.; Goodwin, H. A., Eds.; Springer: Berlin, 2004; p 91.

(15) Reger, D. L.; Gardinier, J. R.; Smith, M. D.; Shahin, A. M.; Long, G. J.; Rebbouh, L.; Grandjean, F. *Inorg. Chem.* **2005**, *44*, 1852.

(16) Reger, D. L.; Gardinier, J. R.; Gemmill, W.; Smith, M. D.; Shahin, A. M.; Long, G. J.; Rebbouh, L.; Grandjean, F. *J. Am. Chem. Soc.* **2005**, *127*, 2303.

(17) (a) Buchen, Th.; Gütlich, P. *Inorg. Chim. Acta* **1995**, *231*, 221. (b) For related work on tris(pyrazolylmethane) complexes, see: Paulsen, H.; Dueland, L.; Zimmermann, A.; Averseng, F.; Gerdan, M.; Winkler, H.; Toftlund, H.; Trautwein, A. X. *Monatsh. Chem.* **2003**, *134*, 295.

(18) De Bari, H.; Zimmer, M. *Inorg. Chem.* **2004**, *43*, 3344.

(19) Long, G. J.; Hutchinson, B. B. *Inorg. Chem.* **1987**, *26*, 608.

Table 1. Crystallographic Properties of $Fe[HB(3,4,5\text{-}Me_3pz)_3]_2$ and $Fe[B(3\text{-}^{cy}Prpz)_4]_2\cdot(CH_3OH)$

complex	$Fe[HB(3,4,5\text{-}Me_3pz)_3]_2$	$Fe[B(3\text{-}^{cy}Prpz)_4]_2\cdot(CH_3OH)$	
formula	$C_{36}H_{56}B_2FeN_{12}$	$C_{49}H_{60}B_2FeN_{16}O$	$C_{49}H_{60}B_2FeN_{16}O$
fw, g/mol	734.40	966.60	966.60
cryst syst	monoclinic	triclinic	triclinic
space group	$C2/c$	$P\bar{1}$	$P\bar{1}$
a, Å	12.9848(7)	12.2356(7)	12.1020(6)
b, Å	18.1300(10)	12.5015(7)	12.1296(6)
c, Å	17.6925(10)	17.8868(10)	17.7576(9)
α, deg	90	87.2590(10)	88.0530(10)
β, deg	110.5150(10)	76.9960(10)	76.9100(10)
γ, deg	90	69.3280(10)	69.4620(10)
V, Å^3	3900.9(4)	2492.7(2)	2374.6(2)
Z	4	2	2
T, K	150(1)	294(1)	90(1)
ρ_{calcd}, Mg m^{-3}	1.250	1.288	1.352
μ (Mo Kα), mm^{-1}	0.429	0.357	0.375
$R[I > 2\sigma(I)]$ (all data)	0.0402 (0.1135)	0.0497 (0.0636)	0.0377 (0.0409)
R_w(all data)	0.0455 (0.1164)	0.1318 (0.1394)	0.1005 (0.1027)

Experimental Section

The $Fe[HB(3,4,5\text{-}Me_3pz)_3]_2$, $Fe[HB(3\text{-}^{cy}Prpz)_3]_2$, $Fe[B(3\text{-}^{cy}Prpz)_4]_2$ (^{cy}Pr = cyclopropyl ring), and $Fe[HB(3\text{-}Mepz)_3]_2$ complexes were prepared according to literature methods.[20,21] Crystals of $Fe[HB(3,4,5\text{-}Me_3pz)_3]_2$ and $Fe[B(3\text{-}^{cy}Prpz)_4]_2\cdot(CH_3OH)$ suitable for X-ray structural studies were grown by layering CH_2Cl_2 solutions of the complexes with CH_3OH and allowing the solvents to slowly diffuse over the course of a few days.

X-ray Structure Determinations. A summary of the crystallographic data and refinement parameters is given in Table 1. X-ray intensity data from a colorless prism of $Fe[HB(3,4,5\text{-}Me_3pz)_3]_2$ were measured at 150(1) K and those from a blocklike crystal of $Fe[B(3\text{-}^{cy}Prpz)_4]_2\cdot(CH_3OH)$ were measured at 294(1) and 90(1) K on a Bruker SMART APEX CCD-based diffractometer with Mo Kα radiation, $\lambda = 0.71073$ Å.[22] Raw data frame integration and Lp corrections were performed with SAINT+.[22] The final unit-cell parameters were determined by least-squares refinement of 8670 reflections from the data set for $Fe[HB(3,4,5\text{-}Me_3pz)_3]_2$ and of 9451 and 6671 reflections of the 90 and 294 K data sets, respectively, for $Fe[B(3\text{-}^{cy}Prpz)_4]_2\cdot(CH_3OH)$ with $I > 5\sigma(I)$. Identical data collections covering full spheres of reciprocal space for $Fe[B(3\text{-}^{cy}Prpz)_4]_2\cdot(CH_3OH)$ were carried out at both temperatures. Analysis of the data showed negligible crystal decay during collection. No absorption correction was applied. Direct methods structure solution, difference Fourier calculations, and full-matrix least-squares refinement against F^2 were performed with SHELXTL.[23] Further details of each data collection and subsequent refinement are given below.

$Fe[HB(3,4,5\text{-}Me_3pz)_3]_2$. $Fe[HB(3,4,5\text{-}Me_3pz)_3]_2$ crystallizes in the $C2/c$ space group, as determined both by the pattern of systematic absences in the intensity data and by the successful solution and refinement of the data. The complex resides on a 2-fold rotational axis. Non-hydrogen atoms were refined with anisotropic displacement parameters; hydrogen atoms were placed in idealized positions and included as riding atoms.

$Fe[B(3\text{-}^{cy}Prpz)_4]_2\cdot(CH_3OH)$. Data were first collected on a colorless crystal at 294 K. The subsequent cooling of the crystal is accompanied by the gradual onset of a pink hue, visibly commencing at ca. 150 K and complete by ca. 125 K; at 90 K, the crystal is purple. With slow cooling, there is no apparent change in the crystal quality or in the unit-cell parameters, other than the expected cell contraction upon cooling. In contrast, flash-freezing the crystals resulted in noticeable cracking.

$Fe[B(3\text{-}^{cy}Prpz)_4]_2\cdot(CH_3OH)$ crystallizes in the triclinic $P\bar{1}$ space group; there is no change in crystal system or space group between 90 and 294 K. The asymmetric unit at each temperature consists of one-half each of two independent $Fe[B(3\text{-}^{cy}Prpz)_4]_2$ complexes, both located on inversion centers, and one methanol molecule. For both data sets, all non-hydrogen atoms were refined with anisotropic displacement parameters; hydrogen atoms bonded to carbon were placed in geometrically idealized positions and included as riding atoms. The methanol O−H proton was located and refined freely at 90 K but could not be located at 294 K. Thus, at 294 K it was included in the position located from the 90 K data and treated as a riding atom for refinement. The rather large displacement ellipsoids of CH_3OH in the 294 K data indicate a mild positional disorder, a disorder that was not modeled.

Magnetic Measurements. The magnetic susceptibilities have been measured at 0.5 T with a Quantum Design MPMS XL SQUID magnetometer. Gelatin capsules were used as sample containers for measurements between 2 and 300 K. The very small diamagnetic susceptibility of these gelatin capsules makes a negligible contribution to the overall magnetization, which was dominated by the sample. The molar magnetic susceptibilities were corrected for the diamagnetism of the complexes; the corrections, which were calculated from tables of Pascal's constants, are -336×10^{-6} emu/mol for $Fe[HB(3\text{-}^{cy}Prpz)_3]_2$ and -565×10^{-6} emu/mol for $Fe[B(3\text{-}^{cy}Prpz)_4]_2$.

Mössbauer Spectra. The Mössbauer spectral absorbers contained ca. 50 mg/cm^2 of crushed but unground powder mixed with boron nitride, and the spectra were measured between 4.2 and 295 K on a constant-acceleration spectrometer which utilized a room-temperature rhodium matrix cobalt-57 source and was calibrated at room temperature with α-iron foil. The estimated relative errors are ±0.005 mm/s for the isomer shifts, ±0.01 mm/s for the quadrupole splittings and line widths, and ±0.2% for the relative spectral absorption areas. The absolute errors are approximately twice as large.

Results

Although magnetic and Mössbauer spectral results for $Fe[HB(3,4,5\text{-}Me_3pz)_3]_2$ have previously shown this complex to be high spin at all temperatures,[14,19] the structure of this

(20) Trofimenko, S. *J. Am. Chem. Soc.* **1967**, *89*, 6288.
(21) Rheingold, A. L.; Yap, G. P.; Liable-Sands, L. M.; Guzei, I. A.; Trofimenko, S. *Inorg. Chem.* **1997**, *36*, 6261.
(22) *SMART Version 5.625*; *SAINT+ Version 6.22*; Bruker Analytical X-ray Systems, Inc.: Madison, WI, 2001.
(23) Sheldrick, G. M. *SHELXTL Version 6.1*; Bruker Analytical X-ray Systems, Inc.: Madison, WI, 2000.

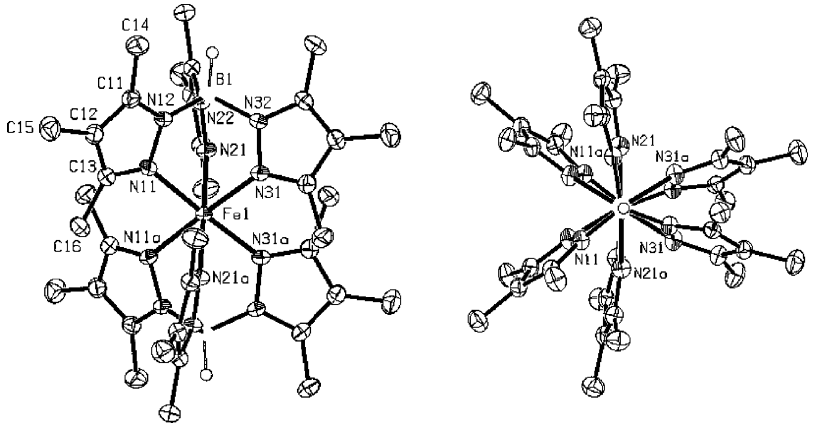

Figure 1. 150 K molecular structure of Fe[HB(3,4,5-Me_3pz)$_3$]$_2$, left, with a view along the C_3 axis, right, that emphasizes the twisting of the pyrazolyl rings.

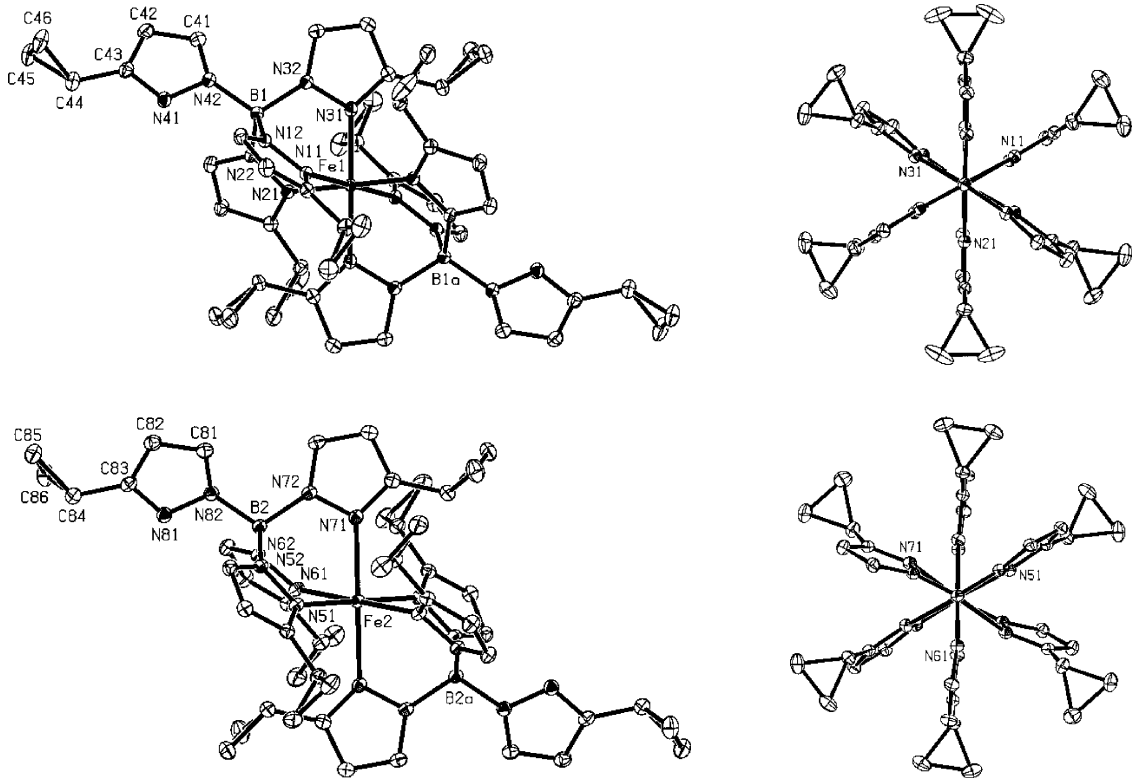

Figure 2. Molecular structure at the Fe1 and Fe2 sites found in Fe[B(3-cyPr)$_4$]$_2$·(CH_3OH) obtained at 90 K. The Fe1 complex, top, is low spin, and the Fe2 complex, bottom, is high spin. The views to the right shown down the C_3 axis (free ^{cy}Pr groups removed for clarity) emphasize the twisting of the pyrazolyl rings.

material remained unknown. Thus, for the purpose of comparison with other closely related complexes, such as Fe[HB(3,5-Me_3pz)$_3$]$_2$, a complex that does undergo a thermally induced SCO, we have determined the molecular structure for Fe[HB(3,4,5-Me_3pz)$_3$]$_2$. Also, although the structure of the toluene solvate of Fe[B(3-^{cy}Prpz)$_4$]$_2$ at ambient temperature has been reported,[21] the temperature dependence of its solid-state structure, magnetic properties, and Mössbauer spectra have not been reported. To carry out these studies and variable-temperature X-ray structural investigations, we crystallized a methanol solvate of Fe[B(3-^{cy}Prpz)$_4$]$_2$. X-ray crystallographic studies at two temperatures were carried out on this solvate, and the magnetic and Mössbauer spectral properties of the desolvated form (these crystals lose solvent on drying) of this new crystalline form were measured.

The 150 K structure of Fe[HB(3,4,5-Me_3pz)$_3$]$_2$ and the 90 K structure of Fe[B(3-^{cy}Prpz)$_4$]$_2$·(CH_3OH) are shown in Figures 1 and 2, respectively; selected bond distances and angles are given in Table 2. In agreement with the magnetic and Mössbauer spectral results,[19] Fe[HB(3,4,5-Me_3pz)$_3$]$_2$ is high spin at 150 K with typical high-spin Fe−N bond distances that average 2.19 Å. The geometry about the iron(II) is a trigonally distorted octahedron; restraints imposed by the chelate rings of each ligand limit the intraligand N−Fe−N bond angles to an average of 86.2°.

Table 2. Selected Bond Distances (Å) and Angles (deg)

	$Fe[HB(3,4,5\text{-}Me_3pz)_3]_2$	$Fe[B(3\text{-}^{cy}Prpz)_4]_2$	$Fe[B(3\text{-}^{cy}Prpz)_4]_2\cdot(CH_3OH)$
temp, K	150	90	294
Fe(1)−N(11)	2.1869(14)	2.0118(11)	2.1984(15)
Fe(1)−N(21)	2.1907(15)	1.9777 (11)	2. 1355(15)
Fe(1)−N(31)	2.1936(15)	2.0091(11)	2.1908(15)
Fe(2)−N(51)		2.1365(11)	2.1537(15)
Fe(2)−N(61)		2.1875(11)	2.1902(14)
Fe(2)−N(71)		2.2106 (11)	2.2145(15)
N(11)−Fe(1)−N(21)	85.66(5)	89.46(4)	85.91(6)
N(21)−Fe(1)−N(31)	87.90(6)	89.66(4)	85.35(6)
N(31)−Fe(1)−N(11)	84.96(6)	89.48(4)	86.75(6)
N(11a)−Fe(1)−N(11)	96.43(7)	180	180
N(21a)−Fe(1)−N(21)	179.02(7)	180	180
N(31a)−Fe(1)−N(31)	93.69(8)	180	180
N(11)−Fe(1)−N(21a)	93.69(5)	90.54(4)	94.09(6)
N(21)−Fe(1)−N(31a)	92.77(5)	90.34(4)	94.65(6)
N(31)−Fe(1)−N(11a)	177.96(5)	90.52(4)	93.25(6)
N(12)−B(1)−N(22)	109.43(14)	108.36(10)	109.24(15)
N(22)−B(1)−N(32)	108.54(14)	109.26(10)	110.50(15)
N(32)−B(1)−N(12)	109.76(15)	106.84(10)	107.96(16)
FeN−NB average torsion angle	20.2	Fe(1) 5.7 Fe(2) 9.3	5.5 10.4

There are two independent molecules in the unit cell of $Fe[B(3\text{-}^{cy}Prpz)_4]_2$ in structures obtained at 294 and 90 K. At 294 K, the average Fe−N distances of 2.17 Å for Fe1 and 2.19 Å for Fe2 clearly indicate that both molecules are in the high-spin state. Upon cooling to 90 K, one of the two iron sites, Fe1, changes from high spin to low spin with an average Fe−N bond distance of 2.00 Å that is typical of low-spin iron(II), whereas the second Fe2 site remains high spin with an average Fe−N bond distances of 2.18 Å.

Supramolecular Structures. The supramolecular structures of all known bis[tris(pyrazolyl)borate]iron(II) complexes reported by us and those deposited in the Cambridge Structural database have been examined in an effort to establish a correlation between their structures and spin-crossover behaviors. Only the newly obtained structures of $Fe[HB(3,4,5\text{-}Me_3pz)_3]_2$ and of $Fe[B(3\text{-}^{cy}Prpz)_4]_2\cdot(CH_3OH)$ will be discussed in detail in this section; the discussion of the remainder of the complexes is included in the Supporting Information and our previous papers.[15,16]

$Fe[HB(3,4,5\text{-}Me_3pz)_3]_2$. The supramolecular structure of $Fe[HB(3,4,5\text{-}Me_3pz)_3]_2$ (Figure 3) is that of interdigitated two-dimensional sheets. The sheets formed in the *ab* plane are a result of CH···π interactions[24] (Figure 3, red lines) that occur between (pyrazolyl)methyl hydrogen donors [CH(36a)] and the π-clouds of the pyrazolyl rings containing N(11) {CH(36a)···Ct[N(11)] 3.00 Å, 149.3°}. There are two donors and two acceptors on each molecule of $Fe[HB(3,4,5\text{-}Me_3pz)_3]_2$ propagating the interaction in two dimensions. The sheets are stacked along *c* such that the methyl groups of the pyrazolyl rings of one sheet fit into the voids found in adjacent sheets.

$Fe[B(3\text{-}^{cy}Prpz)_4]_2\cdot(CH_3OH)$. Three sets of noncovalent NH···O, CH···O, and CH···N interactions serve to organize the two crystallographically independent molecules containing Fe1 and Fe2, respectively, into two-dimensional sheets in both the 90 and 294 K structures of $Fe[B(3\text{-}^{cy}Prpz)_4]_2\cdot(CH_3OH)$ (Figure 4 and Table 3); as expected, the noncovalent interactions are longer at 294 K. The methanol solvent of crystallization serves to bridge alternating Fe1 and Fe2 units to form polymeric chains along the [0,1,−1] direction (Figure 4a, red dashed lines). The hydroxyl hydrogen forms a short hydrogen bond with N(41) of the noncoordinated

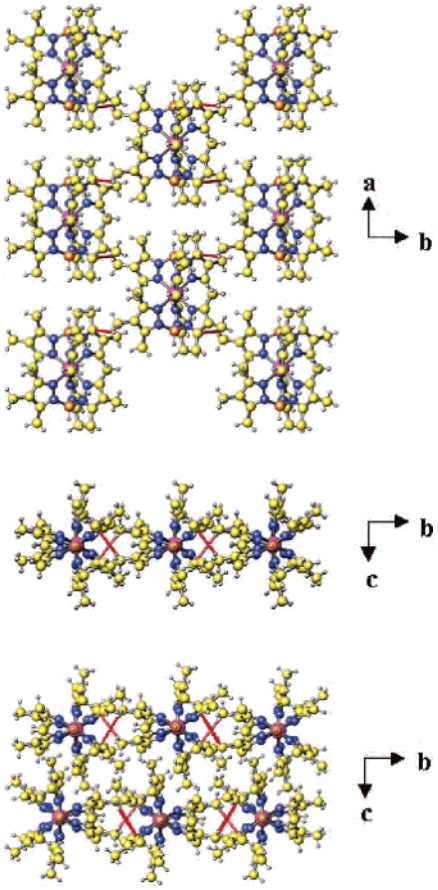

Figure 3. Supramolecular structure of $Fe[HB(3,4,5\text{-}Me_3pz)_3]_2$. Top: View normal to a sheet of molecules held together by CH···π interactions, the red lines. Middle: Side view of a sheet down the *a* axis. Bottom: Stacking of two sheets along the *c* axis.

(24) (a) Takahashi, H.; Tsuboyama, S.; Umezawa, Y.; Honda, K.; Nishio, M. *Tetrahedron* **2000**, *56*, 6185. (b) Nishio, M.; Hirota, M.; Umezawa, Y. *The CH−π Interaction: Evidence, Nature, and Consequences*; Wiley: New York, 1998.

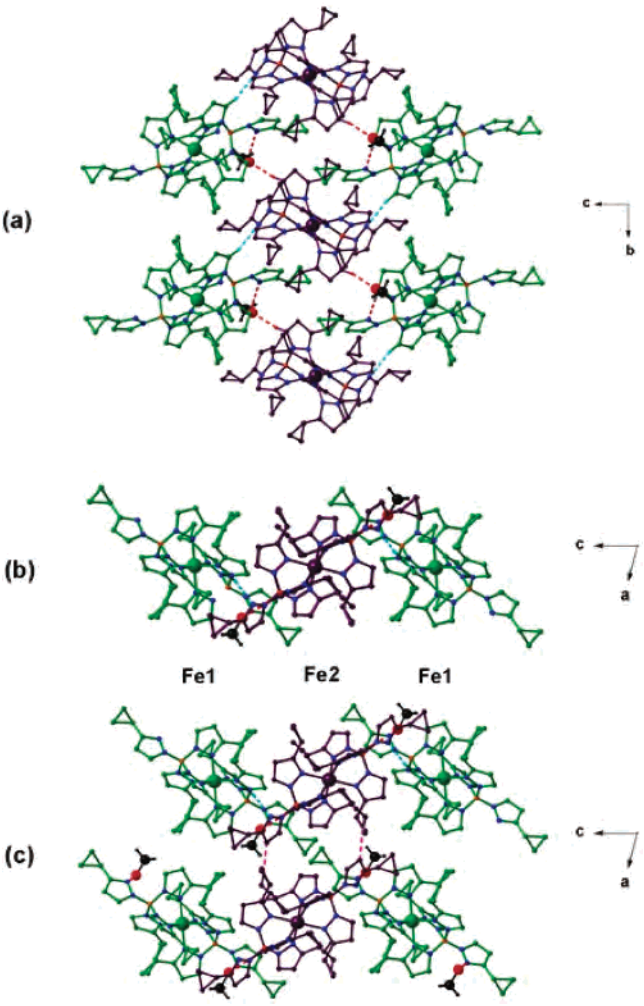

Figure 4. Supramolecular structure of Fe[B(3-^{cy}Prpz)$_4$]$_2$·(CH$_3$OH) at 90 K emphasizing the crystallographically independent molecules containing low-spin Fe1 (green) and high-spin Fe2 (violet). (a) View normal to *bc* sheet structure held together via bridging hydrogen-bonding interactions involving MeOH (red dashed lines) and by weak CH···N interactions between Fe1 and Fe2 (cyan dashed lines). (b) Side view of sheet. (c) Stacking of two sheets held together by very long, weak CH···π bonding interactions (pink dashed lines) between Fe2-containing molecules.

Table 3. Geometry of the Noncovalent Interactions in Fe[B(3-^{cy}Prpz)$_4$]$_2$·(CH$_3$OH)

	H···A, Å		DH···A, deg	
temp, K	294	90	294	90
O(1s)H(1s)···N(41)	2.01	2.00	162	167
C(71)H(71)···O(1s)	2.52	2.43	158	169
C(31)H(31)···N(81)	2.62	2.59	162	166

pyrazolyl in the Fe1 molecule, whereas the methanol oxygen serves as the acceptor in a weak hydrogen-bonding interaction involving an acidic CH donor of a pyrazolyl group bound to Fe2. These polymer chains are assembled into sheets in the *bc* plane by weak hydrogen bonds between an acidic CH of an Fe1-bound pyrazolyl ring and the available nitrogen of the noncoordinating pyrazolyl ring in a neighboring molecule containing Fe2 (Figure 4a, cyan dashed lines). When the sheet is viewed down the *b* axis (Figure 4b), alternating rows of Fe1 and Fe2 are observed. In both the high- and low-temperature structures, the molecules containing Fe2 have additional, but fairly weak, intermolecular contacts (Figure 4c, pink dashed lines). The main interaction is a result of the stacking of the neighboring sheets through rather long, CH···π interaction[24] with the corresponding 90 and 294 K C(55)H(55b)···Ct[N(81)] interaction distances of 3.71 and 3.83 Å and angles of 151° and 166°, respectively.

Magnetic Studies. As mentioned above, the magnetic properties of Fe[HB(3,4,5-Me$_3$pz)$_3$]$_2$ have previously been reported; however, those of the solvent-free Fe[B(3-^{cy}Prpz)$_4$]$_2$ and its structurally characterized relative, Fe[HB(3-^{cy}Prpz)$_3$]$_2$, were unknown prior to this study; the new results obtained herein are shown in Figure 5. For Fe[B(3-^{cy}Prpz)$_4$]$_2$, the measurements were carried out on the desolvated powder that remains after the crystals of Fe[B(3-^{cy}Prpz)$_4$]$_2$·(CH$_3$OH) lose the methanol solvent of crystallization, whereas for Fe[HB(3-^{cy}Prpz)$_3$]$_2$, the magnetic measurements were carried out on its powder. Both complexes exhibit a partial SCO from fully high-spin iron(II) above ca. 150 and 200 K, respectively, to half high-spin and half low-spin iron(II) below 100 K. The behavior is reversible as the samples are heated and recooled. The inverse molar magnetic susceptibility, $1/\chi_M$, of Fe[B(3-^{cy}Prpz)$_4$]$_2$ is linear between 250 and 300 K and a linear least-squares fit yields a Curie constant of 3.285 emuK/mol, a Weiss temperature, θ, of -5.7 K, and a corresponding effective magnetic moment, μ_{eff}, of 5.13 μ_B. Also $1/\chi_M$ of Fe[B(3-^{cy}Prpz)$_4$]$_2$ is linear between 2 and 100 K and yields a Curie constant of 1.700 emuK/mol, a θ of -3.3 K and a corresponding μ_{eff} of 3.69 μ_B. The $1/\chi_M$ of Fe[HB(3-^{cy}Prpz)$_3$]$_2$ is linear between 200 and 300 K and yields a Curie constant of 3.075 emuK/mol, a θ of -5.4 K, and a corresponding μ_{eff} of 4.96 μ_B. Also, $1/\chi_M$ for Fe[HB(3-^{cy}Prpz)$_3$]$_2$ is linear between 2 and 100 K and yields a Curie constant of 1.682 emuK/mol, a θ of -0.64 K and a corresponding μ_{eff} of 3.67 μ_B.

The small observed Weiss temperatures indicate that, as expected, both Fe[B(3-^{cy}Prpz)$_4$]$_2$ and Fe[HB(3-^{cy}Prpz)$_3$]$_2$ are dilute, fully paramagnetic complexes between 2 and 300 K. The moments at the higher temperatures are typical of high-spin iron(II) with a small orbital contribution to the spin-only magnetic moment of 4.90 μ_B. Further, the intermediate moments of 3.67 and 3.69 μ_B are just what would be expected for an iron(II) complex in which one-half of the iron(II) is high spin, with a nominal $^5T_{2g}$ electronic ground state, and the other half is low spin, with a $^1A_{1g}$ electronic ground state. Both the decrease in the moments below ca. 20 K and the slightly negative Weiss temperatures are a result of zero-field splitting of the high-spin iron(II) ground state.

Mössbauer Spectral Studies. Mössbauer spectral data have been reported[19] for Fe[HB(3,4,5-Me$_3$pz)$_3$]$_2$ but not for the 3-cyclopropyl derivatives, nor are complete Mössbauer spectral results available for the closely related *pure* Fe[HB(3-Mepz)$_3$]$_2$.[25] We have undertaken studies on Fe[B(3-^{cy}Prpz)$_4$]$_2$, Fe[HB(3-^{cy}Prpz)$_3$]$_2$, and Fe[HB(3-Mepz)$_3$]$_2$; selected Mössbauer spectra are shown in Figures 6, 7, and 8, respectively. The spectra have been fit with quadrupole doublets with the same line width but, in some cases, with

(25) Calogero, S.; Lobbia, G. G.; Cecchi, P.; Valle, G.; Friedl, J. *Polyhedron* **1994**, *13*, 87.

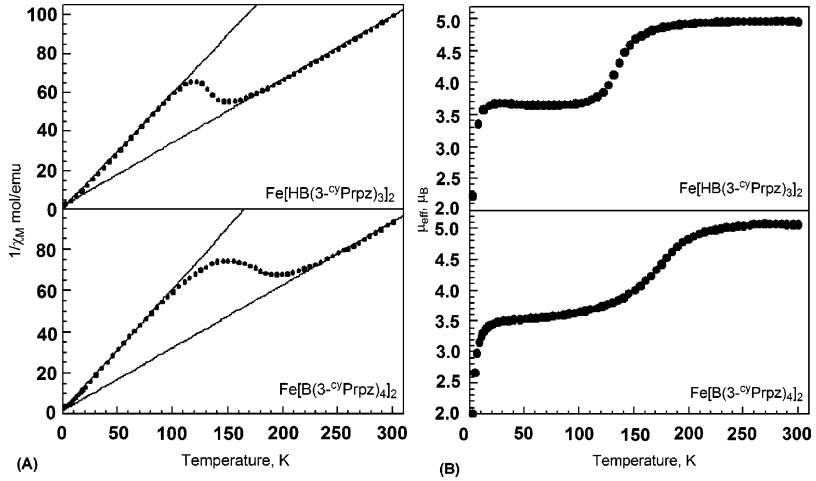

Figure 5. Temperature dependence of the inverse molar magnetic susceptibility (A) and the effective magnetic moment (B) of $Fe[HB(3\text{-}^{cy}Prpz)_3]_2$ and $Fe[B(3\text{-}^{cy}Prpz)_4]_2$.

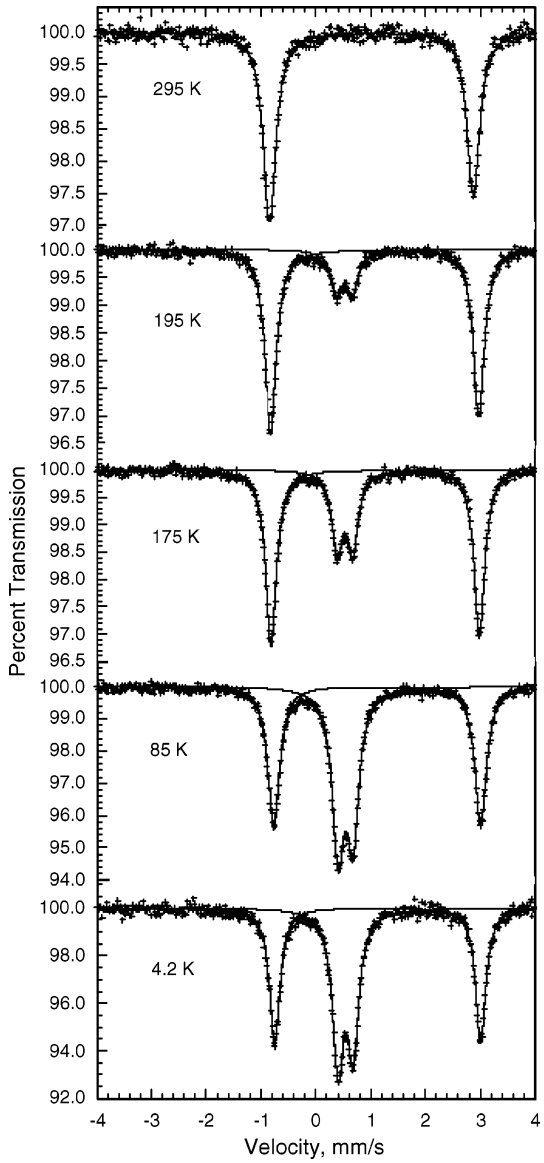

Figure 6. Mössbauer spectra of $Fe[B(3\text{-}^{cy}Prpz)_4]_2$ obtained at the indicated temperatures.

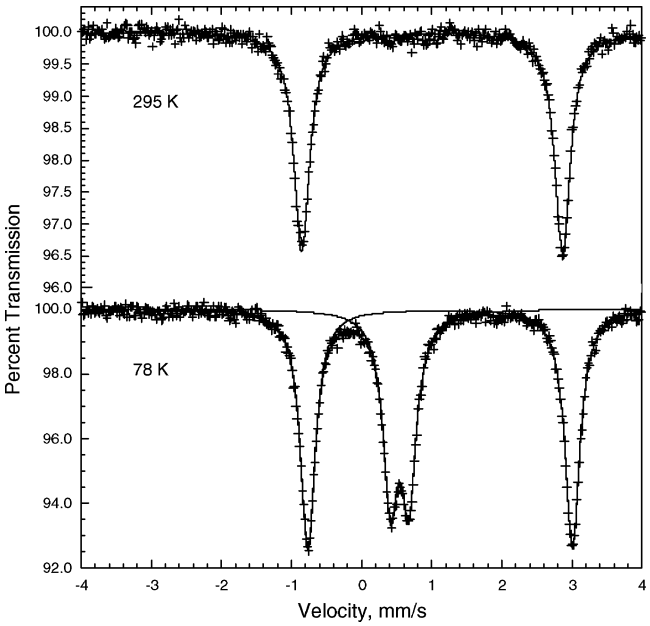

Figure 7. Mössbauer spectra of $Fe[HB(3\text{-}^{cy}Prpz)_3]_2$ obtained at the indicated temperatures.

small differences in the areas of the two components of the doublet, small differences that arise from a small amount of texture in the crushed but unground powder absorber. Selected hyperfine parameters for each complex are given in Table 4, and more extensive results are presented in Table S4 in the Supporting Information.

The Mössbauer spectra of both $Fe[B(3\text{-}^{cy}Prpz)_4]_2$ and $Fe[HB(3\text{-}^{cy}Prpz)_3]_2$ are very similar and are fully consistent with the magnetic results presented above. At room temperature, both complexes are fully high spin with, as expected, very similar hyperfine parameters that are typical[14] of high-spin tris(pyrazolyl)borate complexes. Upon cooling, both complexes undergo a partial SCO to the low-spin state such that at 85 K $Fe[B(3\text{-}^{cy}Prpz)_4]_2$ is 47.5% high spin and at 78 K $Fe[HB(3\text{-}^{cy}Prpz)_3]_2$ is 57.5% high-spin. As is shown in Figure 6, the spectrum of the former complex obtained at 4.2 K is very similar to the 85 K spectrum and shows 46.2% high-spin iron(II). Because of the similarity of their magnetic properties, only the full temperature dependence of the spectra of the $Fe[B(3\text{-}^{cy}Prpz)_4]_2$ complex has been measured. As may be observed at the top of Figure 9, $Fe[B(3\text{-}^{cy}Prpz)_4]_2$

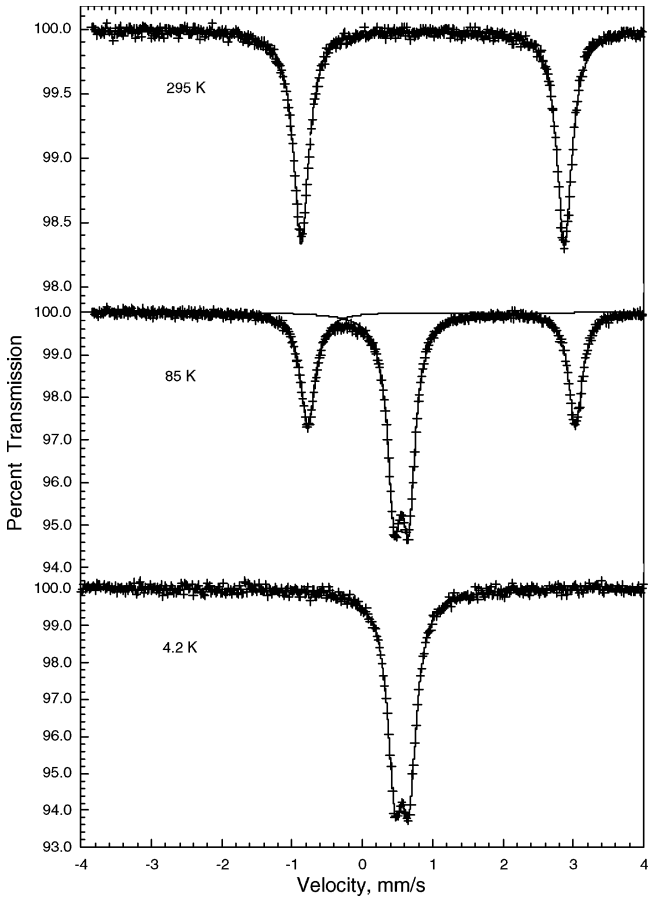

Figure 8. Mössbauer spectra of $Fe[HB(3\text{-}Mepz)_3]_2$ obtained at the indicated temperatures.

undergoes a rather gradual change from fully high-spin above 250 K to approximately one-half low-spin at 130 K, exactly the temperature range over which its effective magnetic moment drops from ca. 5.0 to 3.5 μ_B. The total spectral absorption area and its logarithm, see the lower portion of Figure 9, decrease with increasing temperature because of the decrease in the iron-57 recoil free fraction at higher temperatures. As expected, the quadrupole splittings of both the high-spin and low-spin states exhibit virtually no change with temperature (Figure S10). Further, the small increases in the isomer shifts upon cooling (Figure S11) are exactly those expected of the second-order Doppler shift. The fits shown correspond to Mössbauer temperatures of 470 ± 20 and 640 ± 20 K for the high-spin and low-spin states, respectively, for a nuclide mass or 57 g/mol; as expected, the low-spin state with the shorter Fe−N bond distances has the higher Mössbauer temperature.

In contrast to the above 3-cyclopropyl derivatives, $Fe[HB(3\text{-}Mepz)_3]_2$ exhibits a complete SCO from the high-spin to the low-spin state between 295 and 4.2 K (Figure 8), and the resulting Mössbauer spectral hyperfine parameters are typical of this type of complex (Table 4). It should be noted that the 4.2 K spectrum is different from that reported by Calogero et al.[25] who observed the presence of only 20% of the low-spin state and 58% of the high-spin state at 4.2 K. However, their results are probably influenced by the totally unexpected presence of 22% of a magnetic component, a component that probably indicates that their sample had partially oxidized.

Discussion

An analysis of all known structures of tris- and tetrakis-(pyrazolyl)borate iron(II) complexes reported by us and those deposited in the Cambridge Structural database (see Supporting Information) reveals a number of general spin-state-dependent features of the iron−ligand framework (Tables 5 and 6). Because of the antibonding character of the e_g^* orbitals, high-spin $t_{2g}^4e_g^{*2}$ complexes, such as $Fe[HB(3,4,5\text{-}Me_3pz)_3]_2$, have longer Fe−N distances than low-spin $t_{2g}^6e_g^{*0}$ complexes, such as $Fe[HB(pz)_3]_2$. In high-spin iron(II) complexes, the average Fe−N bond distance is 2.18 Å, a value which is 0.2 Å longer than the 1.98 Å average Fe−N bond distance in low-spin complexes. As a consequence, the FeN_6 octahedral volume averages 13.9 $Å^3$ in the high-spin state but only 10.4 $Å^3$ in the low-spin state. High-spin FeN_6 octahedra tend to be more distorted than low-spin octahedra, as indicated by the greater average high-spin quadratic elongation of 1.005 as compared with a low-spin value of 1.001, where a value of 1.000 represents an undistorted octahedron.[26] The nature of the distortion is either a tetragonal compression or elongation leading to four similar and two mutually opposed, shorter or longer Fe−N bonds. There is no clear correlation between the octahedral distortion and the $T_{1/2}$, the temperature at which half of the iron centers have changed spin-state for the transition in question (Table 6).

For steric reasons, substituents at the 3-positions of the pyrazolyl rings give rise to high-spin complexes at room temperature, with the longer Fe−N bonds that are required to separate the congested scorpionates. In contrast, unsubstituted, uncongested pyrazolyl derivatives are low spin at room temperature. For molecules in the high-spin state, there are clear steric effects that further influence the length of the Fe−N bonds. For example, $Fe[HB(3\text{-}Phpz)_3]_2$ and $Fe[HB(3\text{-}CF_3pz)_3]_2$ have average Fe−N distances of 2.25 and 2.24 Å, respectively, whereas the complexes with smaller 3-substituents, $Fe[HB(3\text{-}^{cy}Prpz)_3]_2$ and $Fe[HB(3\text{-}Mepz)_3]_2$, average ca. 2.20 Å. This metal−nitrogen bond lengthening represents one way that the tris(pyrazolyl)borate ligands can accommodate larger metals, thus favoring the high-spin state. While the longer bond distances in the former complexes with larger substituents prevent SCO, in the latter two cases with similar average Fe−N bond distances, the temperature-dependent spin-crossover behaviors are very different.

We have previously noted, for example, in the case of $Fe[(p\text{-}HC_2C_6H_4)B(3\text{-}Mepz)_3]_2$, that other ligand distortions, namely pyrazolyl ring-twisting, can have a substantial impact on the spin state. After examination of all the iron(II) poly-(pyrazolyl)borate structures, the five different ligand distortions shown in Figure 10 can be identified.

Four of the five distortions, the exception being ring tilting, provide a mechanism for scorpionates with generally fixed bite angles to bind metal ions of different sizes. While ring

(26) Robinson, K.; Gibbs, G. V.; Ribbe, P. H. *Science* **1971**, *172*, 567.

Table 4. Mössbauer Spectral Hyperfine Parameters

complex	T, K	δ,[a] mm/s	ΔE_Q, mm/s	Γ,[b] mm/s	area, %	assignment
$Fe[B(3\text{-}^{cy}Prpz)_4]_2$[c]	295	1.012	3.73	0.26	100	high-spin
	195	1.074	3.80	0.25	81.2	high-spin
		0.521	0.28	0.25	18.8	low-spin
	175	1.085	3.80	0.24	68.8	high-spin
		0.532	0.28	0.24	31.2	low-spin
	85	1.125	3.78	0.24	47.5	high-spin
		0.545	0.28	0.26	52.5	low-spin
	4.2	1.129	3.76	0.23	46.2	high-spin
		0.544	0.28	0.25	53.8	low-spin
$Fe[HB(3\text{-}^{cy}Prpz)_3]_2$	295	1.006	3.72	0.27	100	high-spin
	78	1.122	3.77		57.5	high-spin
		0.544	0.26		42.5	low-spin
$Fe[HB(3\text{-}Mepz)_3]_2$	295	1.010	3.75	0.26	100	high-spin
	85	1.132	3.80	0.24	40.3	high-spin
		0.561	0.20	0.23	59.7	low-spin
	65	1.144	3.81	0.26	16.5	high-spin
		0.560	0.20	0.26	83.5	low-spin
	40	0.562	0.20	0.26	100	low-spin
	4.2	0.566	0.20	0.26	100	low-spin

[a] The isomer shifts are given relative to room-temperature α-iron foil. [b] Γ is the full-width at half-maximum of the line width. [c] Obtained upon initial cooling from 295 to 4.2 K. Essentially, the same results were obtained upon subsequent heating.

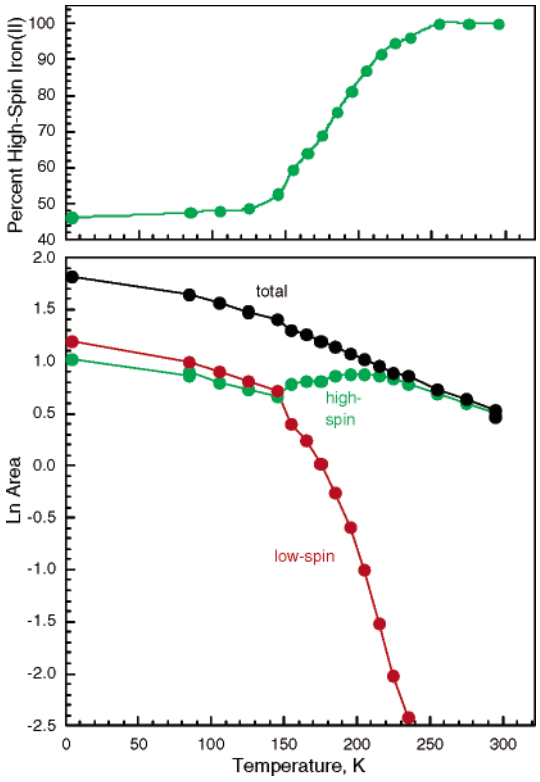

Figure 9. Temperature dependence of the percentage of high-spin iron(II), top, and of the logarithm of the spectral absorption area, bottom, observed for $Fe[B(3\text{-}^{cy}Prpz)_4]_2$.

tilting alone is not expected to influence the size of metal ion that a given scorpionate can bind, or vice versa, this distortion is often coupled with ring-twisting, which does impact the binding of the metal ion. We have formerly used the two terms interchangeably because both remove the mirror planes in the ideal C_{3v}-type arrangement in the ligand. More rigorously, however, ring-twisting can be measured by the FeN−NB torsion angle. A metal-bonded ligand fragment with ideal C_{3v} symmetry is expected to have an FeN−NB torsion angle of 0°. Ring tilting can be measured by the FeN−NC torsion angle, ideally 180°. There can be ring-twisting without tilting, yet twisting will cause the FeN−NC torsion angle to have a value other than 180°; thus, separating the two distortions can be relatively difficult. We will limit further discussion to ring-twisting as measured by the FeN−NB torsion angle, although the two torsion angles do correlate (Table 5).[31]

We have previously shown that the MN−NB torsion angles increase as the size of M, the metal ion, increases.[32] For the complexes considered herein, the ca. 1.98 Å bond distances of the low-spin state of iron(II) appear ideal for the coordination of two tris(pyrazolyl)borate ligands. In these low-spin iron(II) complexes, an "ideal" twist angle of ca. 0° is usually observed.[33] The larger distances in the high-spin iron(II) complexes are frequently accommodated by larger ring-twist angles when compared to the low-spin complexes. This behavior is evident in the 90 K structure of $Fe[B(3\text{-}^{cy}Prpz)_4]_2\cdot(CH_3OH)$ (Figure 2), a complex that contains both a high-spin iron(II) (average Fe−N bond distance = 2.18 Å, average FeN−NB torsion angle = 9.3°) and a low-spin iron(II) (average Fe−N bond distance = 2.00 Å, average FeN−NB torsion angle = 5.7°).

In the 3-substituted complexes with ligands that have a hydrogen as both the fourth group bonded to boron and at the 5-position of the pyrazolyl rings (see below), the degree of ring-twisting in the high-spin iron(II) complexes clearly correlates with the SCO behavior, a correlation that is evident in the structure and properties of $Fe[B(3\text{-}^{cy}Prpz)_4]_2\cdot(CH_3OH)$. Of the two crystallographically independent iron(II) mol-

(27) Oliver, J. D.; Mullica, D. F.; Hutchinson, B. B.; Milligan, W. O. *Inorg. Chem.* **1980**, *19*, 165.
(28) Checchi, P.; Berrettoni, M.; Giorgetti, M.; Lobbia, G. G.; Calogero, S.; Stievano, L. *Inorg. Chim. Acta* **2001**, *318*, 67.
(29) Eichorn, D. M.; Armstrong, W. H. *Inorg. Chem.* **1990**, *29*, 3607.
(30) Sohrin, Y.; Kokusen, H.; Matsui, M. *Inorg. Chem.* **1995**, *34*, 3928.
(31) Frohnapfel, D. S.; White, P. S.; Templeton, J. L.; Ruegger, H.; Pregosin, P. S. *Organometallics* **1997**, *16*, 3737.
(32) (a) Reger, D. L.; Wright, T. D.; Little, C. A.; Lamba, J. J. S.; Smith, M. D. *Inorg. Chem.* **2001**, *40*, 3810. (b) Reger, D. L.; Little, C. A.; Smith, M. D.; Long, G. J. *Inorg. Chem.* **2002**, *41*, 4453.
(33) This ideal distance agrees nicely with that (1.95 Å) calculated in a recent theoretical investigation: Bari, H. D.; Zimmer, M. *Inorg. Chem.* **2004**, *43*, 3344.

Table 5. Geometric Parameters for Iron(II) Poly(pyrazolyl)borate Complexes

ligand	*T*, K	spin state	Fe−N, Å	FeN−NC, deg	FeN−NB, deg	Fe−B, Å	B−Ct_{N_3},[a] Å	Fe−Ct_{N_3},[a] Å	FeN_6 *V*, Å^3	ref
$HB(pz)_3$	294	LS	1.975	177.5	2.9	3.08	0.559	1.174	10.255	27
		LS	1.969	179.1	0.8	3.08	0.555	1.170	10.164	27
$HB(3\text{-}Mepz)_3$	294	HS	2.200	176.7	3.5	3.21	0.523	1.346	14.112	25
		HS	2.208	178.3	0.5	3.23	0.529	1.353	14.272	25
$HB(3,5\text{-}Me_2pz)_3$	294	HS	2.171	174.2	6.8	3.18	0.502	1.326	13.578	27
$HB(3,4,5\text{-}Me_3pz)_3$	150	HS	2.191	162.4	20.2	3.19	0.520	1.346	13.913	this work
$HB(3\text{-}^{cy}Prpz)_3$	294	HS	2.199	179.1	0.3	3.20	0.509	1.354	14.070	21
$HB(3\text{-}CF_3pz)_3$	294	HS	2.236	178.3	1.0	3.15	0.491	1.332	14.875	28
$HB(3\text{-}Phpz)_3$	163	HS	2.246	174.2	7.3	3.11	0.475	1.318	14.923	29
$B(pz)_4$	294	LS	1.961	172.5	3.0	3.09	0.562	1.160	10.049	30
		LS	1.974	175.1	1.7	3.08	0.549	1.173	10.241	30
$B(3\text{-}^{cy}Prpz)_4\,CH_2Cl_2$ solvate	294	HS	2.190	169.0	11.7	3.22	0.522	1.351	13.906	21
		HS	2.184	168.8	9.0	3.20	0.518	1.345	13.790	21
$B(3\text{-}^{cy}Prpz)_4\,CH_3OH$ solvate[b]	294	HS	2.175	171.0	5.5	3.21	0.523	1.340	13.616	this work
		HS	2.186	167.7	10.4	3.22	0.524	1.351	13.816	this work
	90	LS	2.000	174.8	5.7	3.07	0.547	1.164	10.657	this work
		HS	2.179	166.3	9.3	3.20	0.525	1.338	13.677	this work
$(Ph)B(pz)_3$	294	LS	1.987	171.3	5.3	3.15	0.615	1.183	10.141	30
$(Ph)B(3\text{-}Mepz)_3$	294	HS	2.188	162.9	11.8	3.23	0.556	1.346	13.847	35
	90	HS	2.182	162.1	12.9	3.23	0.559	1.343	13.743	35
$(p\text{-}IC_6H_4)B(pz)_3$	150	LS	1.963	172.6	5.0	3.12	0.598	1.166	10.078	15
$(p\text{-}IC_6H_4)B(3\text{-}Mepz)_3{\cdot}2CH_2Cl_2$	200	HS	2.162	164.4	9.8	3.23	0.559	1.327	13.383	15
	100	LS	1.993	171.2	5.3	3.11	0.584	1.161	10.545	15
$(p\text{-}IC_6H_4)B(3\text{-}Mepz)_3$, SCO[c]	294	HS	2.175	166.1	8.6	3.23	0.556	1.334	13.619	15
	200	HS/LS	2.085	168.6	6.9	3.17	0.572	1.247	12.053	15
	100	LS	1.992	171.8	4.8	3.10	0.587	1.157	10.535	15
$(p\text{-}IC_6H_4)B(3\text{-}Mepz)_3$, nSCO[c]	150	HS	2.184	164.9	9.3	3.24	0.553	1.346	13.766	15
$(p\text{-}Me_3SiC_2C_6H_4)\,B(3\text{-}Mepz)_3$	200	HS	2.165	165.4	7.9	3.21	0.553	1.317	13.448	16
$(p\text{-}HC_2C_6H_4)B(3\text{-}Mepz)_3$	294	HS	2.178	164.4	9.2	3.17	0.552	1.324	13.710	16
		HS/LS	2.101	170.2	6.0	3.21	0.568	1.262	12.328	16
	150	HS	2.173	163.5	9.3	3.20	0.546	1.317	13.626	16
		LS	1.988	172.8	4.4	3.09	0.583	1.149	10.469	16
	90	LS	1.994	169.8	5.2	3.08	0.576	1.148	10.576	16
		LS	1.989	172.1	4.8	3.09	0.581	1.149	10.494	16
$(Ph)C_2C_6H_4B(3\text{-}Mepz)_3$	294	HS	2.172	164.7	10.5	3.23	0.553	1.338	13.557	16

[a] Ct_{N_3} is the plane of the three nitrogen atoms bonded to the shown atom. [b] The iron(II) complex of this ligand exhibits a spin-state crossover to 50% high spin and 50% low spin at low temperature. [c] SCO = spin-state crossover, nSCO = no spin-state crossover

Table 6. Crystallographic and Supramolecular Properties of the Iron(II) Poly(pyrazolyl)borate Complexes

ligand	space group, *Z*	spin crossover range, K	$T_{1/2}$[a], K	supramolecular structure	ref
$HB(pz)_3$[b]	$P2_1/c$, 4	280−460	343, 390	3D stacked sheets	27
$HB(3\text{-}Mepz)_3$	$P\bar{1}$, 2	40−85	ca. 85	1D chains	25
$HB(3,5\text{-}Me_2pz)_3$	$P\bar{1}$, 1	150−240	190	1D chains	27
$HB(3,4,5\text{-}Me_3pz)_3$	$C2/c$, 4	none	<4	2D interdig. sheets	this work
$HB(3\text{-}^{cy}Prpz)_3$[c]	$C2/m$, 2	110−160	110	none	21
$HB(3\text{-}CF_3pz)_3$	$P2_1/n$, 2	none	<4	1D chains (w CHF)	28
$HB(3\text{-}Phpz)_3$	$P2_1/n$, 4	−	−	2D sheets	29
$B(pz)_4$	$P\bar{1}$, 2	−	−	3D stacked sheets	30
$B(3\text{-}^{cy}Prpz)_4\,CH_3OH$[c]	$P\bar{1}$, 2	173[d]	173[d]	2D sheets	this work
$(Ph)B(pz)_3$	$Pca2_1$, 4	−	−	3D corr. sheets	30
$(Ph)B(3\text{-}Mepz)_3$	$P\bar{1}$, 1	−	<4	none	34
$(p\text{-}IC_6H_4)B(pz)_3$	$Pbcn$, 4	−	−	2D corr. sheets	15
$(p\text{-}IC_6H_4)B(3\text{-}Mepz)_3\,2CH_2Cl_2$	$P2_1/c$, 2	145−225	185	2D corr. sheets	15
$(p\text{-}IC_6H_4)B(3\text{-}Mepz)_3$, SCO	$P2_1/c$, 2	121−131	126	2D corr. sheets	
$(p\text{-}IC_6H_4)B(3\text{-}Mepz)_3$, nSCO	$P2_1/c$, 2	none	<4	3D stacked sheets	15
$(p\text{-}Me_3SiC_2C_6H_4)B(3\text{-}Mepz)_3$[c]	$P2_1/c$, 2	172−180	175	2D sheets	16
$(p\text{-}HC_2C_6H_4)B(3\text{-}Mepz)_3$	$P2/c$, 4	185−350	280	3D stacked bilayers	16
		106−114	210		
$(p\text{-}PhC_2C_6H_4)B(3\text{-}Mepz)_3$[b]	$C2/c$, 4	200−150	163, 193	3D stacked sheets	16

[a] $T_{1/2}$ is the temperature at which half of the iron centers have changed spin-state for the transition in question. [b] The spin-state crossover (SCO) of the iron(II) complex with this ligand exhibits hysteresis. [c] The iron(II) complex of this ligand exhibits a spin-state crossover to 50% high spin and 50% low spin at low temperature. [d] Desolvated crystals.

ecules in this structure, Fe1, with a 294 K torsion angle of 5.5° in the high-spin state, undergoes a SCO upon cooling. In contrast, Fe2, with a 294 K torsion angle of 10.4° remains high spin upon cooling. This behavior is similar to that observed for $Fe[(p\text{-}HC_2C_6H_4)B(3\text{-}Mepz)_3]_2$, which also has two crystallographically independent iron(II) molecules. In this complex, the Fe1 site, with an FeN−NB torsion angle of 9.2° at 294 K undergoes a SCO at 110 K, whereas the Fe2 site with an FeN−NB torsion angle of 6.0° at 294 K undergoes a spin-state transition between 200 and 300 K.

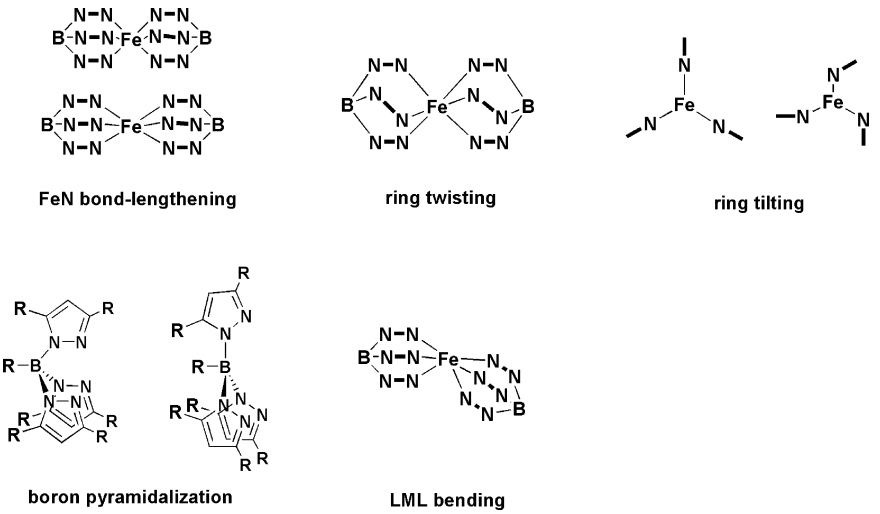

Figure 10. Common ligand distortions in iron(II) poly(pyrazolyl)borates, where N−N represents a pyrazolyl ring.

More generally, upon cooling an iron(II) site with less pyrazolyl ring-twisting, i.e., a smaller FeN−NB torsion angle, can relax to the low-spin state more easily and thus at a higher temperature because its structure is already more like that observed in the low-spin tris(pyrazolyl)borate iron(II) complexes. In contrast, it takes a lower temperature for the pyrazolyl rings with greater twisting, i.e., a larger FeN−NB torsion angle, to switch to the low-spin state.[34] This influence of the FeN−NB torsion angle is also responsible for the vastly different SCO behavior of the two closely related, methyl-substituted, $Fe[HB(3,4,5\text{-}Me_3pz)_3]_2$ and $Fe[HB(3,5\text{-}Me_2pz)_3]_2$ complexes. The former complex does *not* undergo SCO, whereas the latter does. This difference may be attributed to the FeN−NB torsion angle of 20.2° observed in $Fe[HB(3,4,5\text{-}Me_3pz)_3]_2$, the largest FeN−NB torsion angle found in Table 5. In contrast, the FeN−NB torsion angle in $Fe[HB(3,5\text{-}Me_2pz)_3]_2$ is only 6.8°. The importance of this torsion angle is also exemplified by the fact that $Fe[(Ph)B(3\text{-}Mepz)_3]_2$ does *not* undergo a SCO upon cooling[35] and has large FeN−NB torsion angles of 11.8° and 12.9° at 294 and 90 K, respectively. Thus, for high-spin iron(II) complexes, a room-temperature FeN−NB torsion angle of ca. 11° or larger appears to be the limit above which a SCO to the low-spin state will *not* occur upon cooling.

A detailed structural analysis also indicated that another way for scorpionate ligands to accommodate metal ions of different sizes is to change their bite angle through a pyramidal deformation about boron. In this deformation, the B−N bond distances and B−N−N angles remain constant and the N−B−N bond angles change. This deformation at boron can be quantized in terms of the distance from the boron to the centroid of the B−N-bonded N_3 plane ($B-Ct_{N_3}$), a distance that varies from 0.48 to 0.62 Å (Table 5). An increase in the pyramidal distortion, i.e., a decrease in $B-Ct_{N_3}$, moves the boron closer to the mean plane of the boron-bound nitrogens, as is shown at the bottom left of Figure 10. This deformation is most important for ligands that have a hydrogen as both the fourth group bonded to boron and at the 5-position of the pyrazolyl rings. Steric interactions prevent the pyramidal deformation in ligands that have a pyrazolyl or phenyl ring as the fourth group bonded to boron *or* that have substituents at the 5-position of the three pyrazolyl rings. For these ligands, a ring-twist dominates over the pyramidal deformation at boron. For example, even though both of the average Fe−N bond distances of 2.18 Å observed in the high-spin polymorphs of $Fe[(p\text{-}IC_6H_4)B(3\text{-}Mepz)_3]_2$ are shorter than the 2.20 and 2.21 Å distances found in $Fe[HB(3\text{-}Mepz)_3]_2$, the Fe···B distance in each is ca. 3.23 Å. These surprisingly constant values are made possible by pyrazolyl ring-twisting in the former but not in the latter complex, but in this latter case, the pyramidal deformation is observed. The overall result of the deformation is that the hydrogen atoms at the 5-position of the pyrazolyl rings are pushed toward the H−B bond, thus increasing the three bidentate "bites" of the ligand and producing longer Fe−N bond distances. In high-spin $Fe[HB(3\text{-}Mepz)_3]_2$, the borons in the two independent molecules are 0.52 and 0.53 Å above the center of the N_3 planes and have average B−N−N angles of 121.9° and 121.3°, respectively. In the two polymorphs of $Fe[(p\text{-}IC_6H_4)B(3\text{-}Mepz)_3]_2$, the borons are farther above the N_3 planes at 0.55 and 0.56 Å but the associated B−N−N average angles of 121.2° and 121.5°, respectively, are nearly the same. Thus, the conformational flexibility of $[HB(3\text{-}Rpz)_3]^-$ ligands permits binding to larger metal ions through a pyramidal deformation at boron. However, steric interactions involving the hydrogen atoms at the 5-position of the three pyrazolyl rings and the atoms of the aryl group in the $(p\text{-}IC_6H_4)B(3\text{-}Mepz)_3$ moiety direct the deformation of the ligand such that the pyrazolyl rings *must* twist to accommodate binding to larger metal ions.

From the limited data available, we believe that there may be a correlation between the pyramidal deformation at boron and the $T_{1/2}$ of the SCO. This correlation is exemplified in the complexes that have a H−B bond and a hydrogen in the

(34) These results parallel those observed for $\{Fe[HC(3,5\text{-}Me_2pz)_3]_2\}(BF_4)_2$ in which a phase change caused a large increase of the pyrazolyl ring-twisting for one of the sites, the site that did not undergo spin crossover at low temperature, and actually decreased the twisting at the other site, forcing a highly cooperative changeover: Reger, D. L.; Little, C. A.; Young, V. G.; Pink, M. *Inorg. Chem.* **2001**, *40*, 2870.

5-position of the three pyrazolyl rings, i.e., in Fe[HB(3-CF_3-pz)$_3$]$_2$, Fe[HB(3-Mepz)$_3$]$_2$, Fe[HB(3-^{cy}Prpz)$_3$]$_2$, and Fe[HB-(pz)$_3$]$_2$. In these complexes, the FeN−NB torsion angles are of a similar order of magnitude, averaging 1.0°, 2°, 0.3°, and 1.9°, respectively. The corresponding B−Ct_{N_3} distances are 0.49, 0.53, 0.51, and 0.56 Å, and the corresponding $T_{1/2}$ temperatures are <4, 85, 110, and 390 K, respectively. The observed values for Fe[HB(3-^{cy}Prpz)$_3$]$_2$ appear out of line but may be unique in this series because this complex undergoes an unexpected 50% SCO that presumably is induced by a phase transition occurring at the relatively low temperature of 110 K. When compared with Fe[B(3-^{cy}-Prpz)$_4$]$_2$·(CH_3OH), in which there are two independent iron-(II) sites, the partial changeover in Fe[HB(3-^{cy}Prpz)$_3$]$_2$ is unexpected because the crystalline form studied by X-ray crystallography has a unique iron(II) site. We have previously reported[36] on a similar behavior in {Fe[HC(3,5-Me_2pz)$_3$]$_2$}-(BF_4)$_2$, a complex that also has a crystallographically unique iron(II) site in the room temperature X-ray structure. In this complex, a crystallographic phase transition causes a similar change from 100% high-spin iron(II) at 295 K to 50% high-spin and 50% low-spin below ca. 205 K. Probably because of their ionic lattice, the crystals of {Fe[HC(3,5-Me_2pz)$_3$]$_2$}-(BF_4)$_2$ did not shatter at the phase transition, and as a consequence, their low-temperature structures could be obtained. Although it is hard to prove crystallographically, crystal fracturing or shattering associated with a phase transition is common in molecular SCO complexes of the borates, such as Fe[HB(3-^{cy}Prpz)$_3$]$_2$, Fe[(*p*-$PhC_2C_6H_4$)B(3-Mepz)$_3$]$_2$,[16] or Fe[(*p*-$Me_3SiC_2C_6H_4$)B(3-Mepz)$_3$]$_2$.[16]

The final type of ligand−metal bonding distortion, ligand−metal−ligand, or L−M−L, bending (see the bottom right of Figure 10) does not appear to be important as the largest distortion is with Fe[HB(3-Phpz)$_3$]$_2$, where the B···Fe···B angle, is 177°.

Following our previous studies on the different SCO behavior of different polymorphs of Fe[(*p*-IC_6H_4)B(3-Mepz)$_3$]$_2$, we have examined the impact of crystal packing and supramolecular structure on the SCO behavior of the iron(II) poly(pyrazolyl)borates. We had envisioned that highly organized three-dimensional structures could have a significant impact on the spin-crossover behavior. We have clearly demonstrated this effect with the two polymorphs of Fe[(*p*-IC_6H_4)B(3-Mepz)$_3$]$_2$. They both have very similar ligand distortions, but one polymorph has a highly organized three-dimensional supramolecular structure and does not undergo a SCO upon cooling to 4 K. The second polymorph of Fe[(*p*-IC_6H_4)B(3-Mepz)$_3$]$_2$ has a stacked two-dimensional supramolecular structure, a structure that is clearly less well organized than that of the other polymorph, and undergoes an abrupt iron(II) SCO from high spin to low spin upon cooling below ca. 130 K. Careful examination of the complexes in Tables 5 and 6, for which variable temperature X-ray data are available or magnetic and/or Mössbauer spectral properties are known, indicates that there is no simple correlation between the crystal system or space group of a given SCO complex and the $T_{1/2}$ of the SCO or the occurrence of magnetic hysteresis. Furthermore, there is no clear additional instance where the supramolecular structure impacts the SCO behavior. The best possible case is in the structure reported here for Fe[B(3-^{cy}Prpz)$_4$]$_2$·(CH_3OH) where there are two independent molecules in the unit cell but only one undergoes a SCO. In this case, there are more intermolecular contacts that are 0.1 Å less than the sum of the van der Waals radii involving the Fe2 molecule than there are for the Fe1 molecule. This difference could be responsible for the different SCO behavior of the two molecules; the Fe2 being more bound into the lattice, thus requiring a lower temperature to induce the SCO. Coincidentally, the Fe2 molecule has greater pyrazolyl-twisting than does the Fe1 molecule, a twisting which, as outlined above, would also be expected to resist the SCO upon cooling. In this instance, it is more likely that the pyrazolyl ring-twisting dominates the SCO because of the seemingly weak nature of the intermolecular contacts. However, it should be noted that it remains unclear the extent to which the crystal packing influences the extent of the pyrazolyl ring-twisting. The influence of the supramolecular structure, although not a dominating factor in controlling the SCO, has proven to be a viable mechanism for fine-tuning the spin-state change and warrants further study.

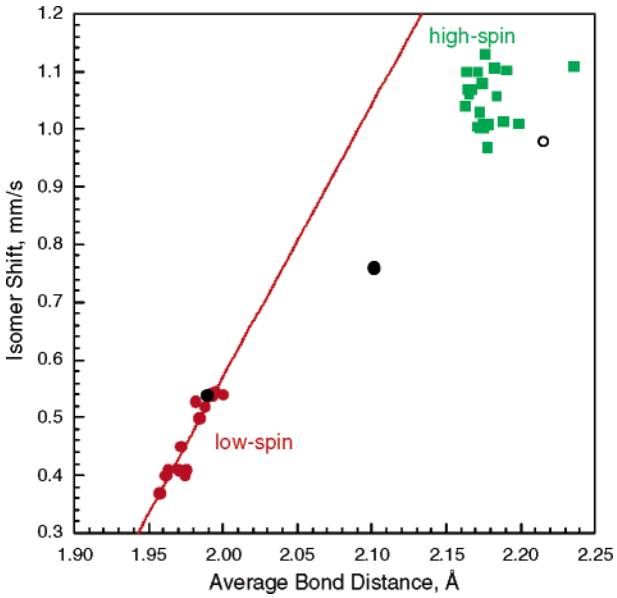

Figure 11. Correlation between the isomer shift and the average Fe−N bond distance in the iron(II) pyrazolylborate complexes. The black points corresponds to the Fe2 site in Fe[(*p*-$HC_2C_6H_4$)B(3-Mepz)$_3$]$_2$. The error bars are at most the size of the symbols.

This study has also revealed unexpected correlations between the Mössbauer spectral properties and Fe−N bond lengths, distortions, and even the pyrazolyl ring distortions. First, there is a correlation between the Mössbauer-effect isomer shift and the average Fe−N bond distance in the low-spin iron(II) complexes (Figure 11). As expected, as the bond distance increases, the s-electron density at the nucleus decreases and the isomer shift increases. Although the longer

(35) Reger, D. L.; Elgin, J. D.; Smith, M. D.; Grandjean, F.; Rebbouh, L.; Long, G. J. *Polyhedron* **2006**, doi: 10.1016/j.poly.2006.03.014.
(36) Reger, D. L.; Little, C. A.; Smith, M. D.; Long; G. L. *Inorg. Chem.* **2002**, *41*, 4453.

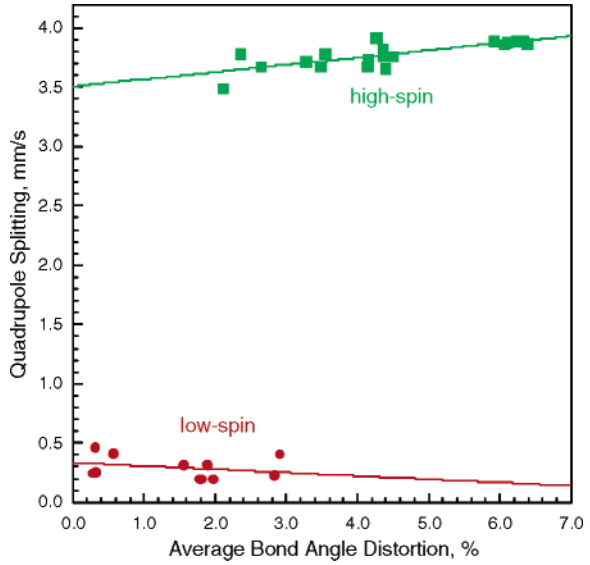

Figure 12. Correlation between the quadrupole splitting and the average N−Fe−N intraligand bond angle distortion in the iron(II) pyrazolylborate complexes. The error bars are at most the size of the symbols.

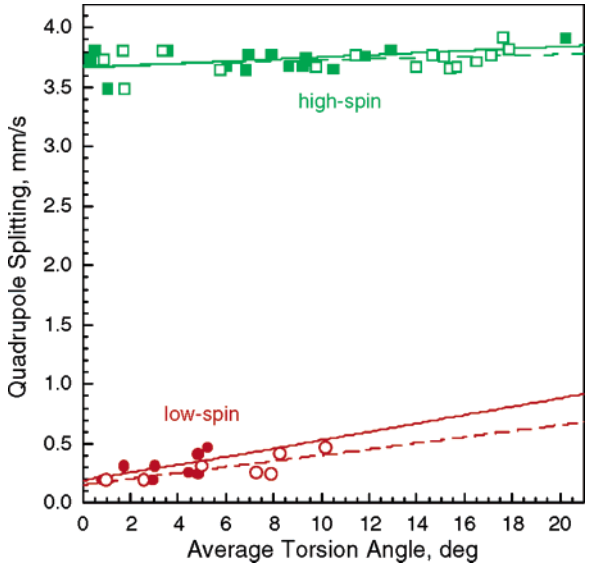

Figure 13. Correlation between the quadrupole splitting and the supplement of the average intraligand FeN−NC torsion angles, open symbols and dashed lines, and the average intraligand FeN−NB torsion angles, solid symbols and solid lines. The error bars are at most the size of the symbols.

bond distances of the high-spin complexes leads to substantially larger isomer shifts, there seems to be little correlation of the individual high-spin iron(II) isomer shifts with the average Fe−N bond distance. The failure of the green points for the high-spin state to fall on the red line in Figure 11 is a result of the very different bonding properties of the iron(II) antibonding e_g^* orbitals, orbitals that are only occupied in the high-spin iron(II).

All of the green and red points in Figure 11 correspond to iron(II) pyrazolylborate complexes undergoing a SCO upon cooling. In contrast, the two solid black points in this figure correspond to the Fe2 crystallographic site in Fe[(*p*-$HC_2C_6H_4$)B(3-Mepz)$_3$]$_2$, the only iron(II) site undergoing a spin-state transition[16] (i.e., a temperature range where the SCO compound is neither fully high spin nor fully low spin) in the pyrazolylborate complexes under study herein. At 90 K, this Fe2 is low-spin and has an isomer shift of 0.54 mm/s and an average Fe−N bond distance of ca. 1.989 Å, data that match the other low-spin complexes. However, at 294 K, this Fe2 is 51% high-spin with an average Fe−N bond distance of ca. 2.101 Å. Because of the spin-state transition, the Fe2 isomer shift at 294 K is the weighted average of the limiting high-spin and low-spin isomer shifts of 0.980 and 0.531 mm/s, i.e., 0.764 mm/s, used in the spin-state relaxation fits.[16] The two solid black points in Figure 11 correspond to the 90 and 294 K Fe2 results, and a linear extrapolation from these two points to the limiting high-spin isomer shift of 0.98 mm/s, the open black point in Figure 11, indicates that, when the Fe2 site in Fe[(*p*-$HC_2C_6H_4$)B(3-Mepz)$_3$]$_2$ is fully high-spin at 380 K, we can predict it would have an average Fe−N bond distance of ca. 2.215 Å.

There is also a weak but real correlation of the quadrupole splittings with the average N−Fe−N intraligand bond angle distortion in several pyrazolylborate and pyrazolylmethane iron(II) complexes (Figure 12). In this figure, the percentage intraligand bond angle distortion has been defined[37,38] as in eq 1,

$$\%\ \text{distortion} = \frac{100}{n}\sum_{i=1}^{n}\frac{|a_i - a_m|}{a_m} \qquad (1)$$

where n is the number of angles (three), a_i is each individual N−Fe−N intraligand bond angle, and a_m is the average of these angles. It should be noted that, as the distortion of a high-spin iron(II) complex increases, the quadrupole splitting increases, whereas that of a low-spin iron(II) complex decreases, at least slightly. The difference in the sign of the two slopes in Figure 12 arises because the principal components, V_{zz}, of the electric field gradient for the high-spin and low-spin states have different signs.[16]

Finally, the correlation of the Mössbauer-effect quadrupole splittings with the average FeN−NC and FeN−NB intraligand dihedral torsion angles in the iron(II) pyrazolylborate complexes (Figure 13) have been determined for the complexes of the ligands listed in Table 5. To compare the FeN−NC and the FeN−NB torsion angles, the supplement of the former angles has been used in Figure 13. Thus, in each case, a zero distortion corresponds to the highly symmetric configuration in which each of the six pyrazolyl rings in a complex are oriented at 180°, yielding a 3-fold axis with D_{3d} symmetry if the substituents on the ring are ignored. As would be expected, because the low-spin quadrupole splitting is determined by the lattice contribution to the iron(II) electric field gradient, the low-spin quadrupole splitting increases with the average torsion

(37) Renner, B.; Lehmann, G. *Z. Krist.* **1986**, *175*, 43.
(38) Hatert, F.; Long, G. J.; Hautot, D.; Fransolet, A.-M.; Delwiche, J.; Hubin-Franskin, M. J.; Grandjean, F. *Phys. Chem. Miner.* **2004**, *31*, 487.

angle. In contrast, the high-spin quadrupole splitting shows little, if any, correlation with the FeN−NB average torsion angle.

Conclusions

There are now a rather large number of iron(II) complexes with the various derivatives of the pyrazolylborate and pyrazolylmethane ligands whose single-crystal X-ray structures and magnetic and Mössbauer spectral properties are known.[14−16] A number of factors that influence the spin-crossover behavior of this class of complexes are apparent from the various new results reported herein and the collected earlier results. The first and most obvious factor is the steric congestion induced by substitution at the 3-position of the pyrazolyl ring, a congestion that yields longer Fe−N bond distances and high-spin iron(II). A second important feature influencing the iron(II) spin-state is the presence of a substituent other than hydrogen as the fourth substituent on boron or at the 5-position of the pyrazolyl rings. In the absence of these substitutions, the tris(pyrazolyl)borate and tris(pyrazolyl)methane ligands can accommodate changes in different iron(II) spin-states, or more generally accommodate metal ions of different size by pyramidalization, a deformation that opens the ligand bite angle, of boron or central carbon, respectively. It seems that this deformation is not sterically possible with the substituted ligands. Unfortunately, studies of additional complexes will be needed to correlate this deformation with the $T_{1/2}$ of the SCO.

For complexes with ligands which are substituted on the fourth position of boron or at the 5-position of the pyrazolyl ring, a number of distortions in the coordination sphere can be induced either intramolecularly or imposed by different crystal-packing behaviors. In the complexes studied to date, the intramolecular distortions clearly predominate over intermolecular interactions. Pyrazolyl ring-twisting is the predominant deformation controlling the SCO behavior of these iron(II) complexes. The available structural results indicate that the intrinsic bite angle of the tris(pyrazolyl)-borate and methane ligands is ideally suited to low-spin iron(II) with an Fe−N bond distance of ca. 2 Å.[33] In these low-spin iron(II) complexes, twisting of the pyrazolyl rings is unnecessary, but with the high-spin iron(II) complexes with longer Fe−N bond distances of ca. 2.2 Å, pyrazolyl ring-twisting may well be significant. It seems that complexes having a twist angle of ca. 11° or more in the high-spin iron(II) state at room temperature will not undergo a SCO upon cooling; these complexes are significantly distorted from the ideal low-spin coordination geometry and resist any SCO. Thus, iron(II) poly(pyrazolyl)borate complexes provide a unique opportunity for delineating how subtle *intramolecular* geometrical changes control SCO.

Intermolecular or supramolecular forces are also potentially important in controlling the SCO but can only be identified in cases in which all the molecules in a lattice have similar intramolecular arrangements. For the poly(pyrazolyl)borate complexes studied herein, the polymorphs of Fe[(*p*-IC_6H_4)B-(3-Mepz)$_3$]$_2$ are the only system where we can clearly identify supramolecular forces as controlling the spin-crossover behavior. We plan future studies of these interactions by preparing complexes with stronger supramolecular forces.

The uncontrollable influence of phase changes is clearly a dominant force in the SCO behavior in many of these complexes. For example, the complexes with 3-methyl and 3-cyclopropyl substitutions, both of which have similar steric effects,[21] have very different SCO properties. Fe[B(3-Mepz)$_4$]$_2$ exhibits a complete SCO at low temperature, whereas Fe[B(3-^{cy}Prpz)$_4$]$_2$ and Fe[HB(3-^{cy}Prpz)$_3$]$_2$ both exhibit a 50% changeover. In the latter cases, the crystals shatter at the temperature of the onset of SCO, indicating a phase change. Clearly, phase changes dominate or change the impact of the more subtle influences of ring-twisting and the relatively weak supramolecular interactions that are present in these complexes.

Finally, it has been found that the Mössbauer spectral properties of iron(II) SCO complexes provide insight into the ligand environment in cases where X-ray structural results cannot be obtained; a correlation between the isomer shift with the average Fe−N bond distance has been observed. In addition, observed correlations between the quadrupole splitting and the average FeN−NB intraligand torsion angles and the average N−Fe−N intraligand bond angle distortions are helpful in providing further insight into structural distortions when X-ray structural results are unavailable.

Acknowledgment. The authors acknowledge with thanks the financial support of the U.S. National Science Foundation through Grant No. CHE-0414239 for D.L.R. We thank Jerry Trofimenko for his generous gift of samples of Fe[B(3-^{cy}Prpz)$_4$]$_2$, Fe[HB(3-^{cy}Prpz)$_3$]$_2$, and Fe[HB(3-Mepz)$_3$]$_2$ and Ms. Leila Rebbouh for her help in obtaining the Mössbauer spectra.

Note Added after ASAP Publication. One of the values in Table 4 was incorrect in the version published ASAP August 1, 2006; the corrected version was published August 2, 2006.

Supporting Information Available: Figures, tables, and discussion concerning supramolecular structures of nine different iron(II) bis[poly(pyrazolyl)borates]; extended Mössbauer hyperfine parameters; the temperature dependence of the isomer shifts and quadrupole splittings; and crystallographic information files of the newly characterized complexes in this study. This material is available free of charge via the Internet at http://pubs.acs.org.

IC0607437